Journal of Alloys and Compounds 777 (2019) 8–17

Contents lists available at ScienceDirect

Journal of Alloys and Compounds

journal homepage: http://www.elsevier.com/locate/jalcom

Reactive synthesis of hexagonal $Ti_5P_{3.16}$ crystals and their heterogenous nucleating mechanism on primary Si

Jinfeng Nie [a, *], Yonghao Zhao [a], Yusheng Li [a], Fang Wang [a], Huabing Yang [b], Kaiqi Hu [b], Guiliang Liu [b], Xiangfa Liu [b, **]

[a] Nano and Heterogeneous Materials Center, School of Materials Science and Engineering, Nanjing University of Science and Technology, Nanjing, 210094, China

[b] Key Laboratory for Liquid–Solid Structural Evolution and Processing of Materials, Ministry of Education, Shandong University, Jinan, 250061, China

ARTICLE INFO

Article history:
Received 16 May 2018
Received in revised form
30 August 2018
Accepted 3 September 2018
Available online 6 September 2018

Keywords:
$Ti_5P_{3.16}$
AlP
Al–Si alloy
Primary Si
Refinement
Phase transition

ABSTRACT

Reactive synthesis of $Ti_5P_{3.16}$ crystals was firstly investigated in the Al–Ti–P–C alloy and their effective refinement on primary Si in Al–Si alloys was also revealed. It was found that the $Ti_5P_{3.16}$ phase was formed by the direct reaction of P atoms with TiC particles in Al melt. During the reaction process, P atoms absorbed on TiC agglomerates and initiated the gradual phase decomposition, and then the releasing Ti atoms combined surrounding P ones together to form Ti-P phase. Based on the TEM and SEM characterization, it is identified that the $Ti_5P_{3.16}$ phase has an hexagonal close packed crystal lattice structure and mainly displays a regular hexagonal prism morphology enclosed by six {10-10} facets and two parallel {0001} ones. Furthermore, the Al–Ti–P–C alloy containing the $Ti_5P_{3.16}$ particles showed an efficient refinement performance on primary Si particles for hypereutectic Al–Si alloy, whose average size was reduced from 85 μm to 12.5 μm for A390 alloy. In order to reveal the refinement mechanism, the evolution process of the $Ti_5P_{3.16}$ phase induced by Si atoms in the Al–Si melt was carried out, indicating that the $Ti_5P_{3.16}$ transformed into amounts of nano AlP particles with sizes of about 100–200 nm after added into the melt. Then, these in-situ AlP particles with fresh interfaces distributed uniformly in the melt and act as the effective heterogenous nuclei for the primary Si during the following solidification process of Al–Si melt with the decrease of the melt temperature, which leads to significantly refinement of the microstructure of A390 alloys.

1. Introduction

Al–Si alloys are the most widely used Al based casting alloys, and constitute ~90% of all shape castings [1]. Hypereutectic Al–Si alloys as the appropriate material for pistons of gas engines have been paid considerable attention due to their excellent wear and corrosion resistance, low density, low coefficient of thermal expansion and outstanding mechanical properties [2–4]. However, the coarse and brittle primary Si in the hypereutectic Al–Si alloys can fracture within the soft Al matrix seriously leading to poor mechanical properties. Therefore, the primary Si particles must be refined to improve the mechanical properties of the alloys [5,6]. Up to now, many studies have been carried out to develop effective refiners and reveal the refinement mechanism to meet the increased requirements of industry applications [7–13].

Primary Si can be refined by AlP phase, which is generally accepted as the perfect nucleating site for Si due to its excellent lattice match with Si [14–17]. Several kinds of Al–P alloys containing AlP phase have been widely applied to the Al–Si alloys because of the excellent refining performance [7,18,19]. AlP particles act as the direct nuclei of primary Si and then refines the primary Si during solidification process. It has been revealed that after the Al–P master alloy is added to the Al–Si melt, the coarse AlP particles can dissolve into the melt and new small sized AlP particles will re-precipitate during solidification, which exhibit higher refining efficiency due to their finer size and fresh interface without any foreign substance [24]. However, the refining efficiency of the Al–P master alloys needs to be improved further, due to the re-

* Corresponding author.
** Corresponding author. Key Laboratory for Liquid-Solid Structural Evolution and Processing of Materials, Ministry of Education, Shandong University, No. 17923 Jingshi Road, Jinan, 250061, China.
E-mail addresses: niejinfeng@njust.edu.cn (J. Nie), xfliu@sdu.edu.cn (X. Liu).

https://doi.org/10.1016/j.jallcom.2018.09.038
0925-8388/

precipitation process of AlP is controlled by the equilibrium constant of the dissolution reaction AlP→Al+P, leading to the low refining efficiency. For the Cu–P master alloy, it is easy to fall down to the bottom of the melt and precipitate due to its high density, leading to unstable modification efficiency. Recently, it was found that some other new master alloys such as Al–Zr–P, Al–Sc–P, Al–La–P also had a good refinement effect on primary Si for the near eutectic and hypereutectic multicomponent Al–Si alloys [8,10,20–22]. Also, the ZrP/ReP/ScP phase can react with Si and Al atoms to form in-situ AlP particles in the Al–Si melt [10,22,23]. However, the cost of those transition metals and rare earth elements is relatively high, which limits the wide application of these refiners. Therefore, it is necessary to develop new refiners for Al–Si alloys with higher refining efficiency and lower cost.

It is well known that TiC as a kind of important ceramic material has received increasing attention because of their excellent physical and mechanical properties [25]. It is widely used as refractory materials for cutting tools and wear resistant components, especially as reinforcing phase in composites [26,27]. Al–Ti–C master alloys containing TiC particles are also good grain refiners for Al alloys, because TiC particles are effective nucleating substrates for α-Al grains during the solidification process [28,29]. However, many studies have revealed that TiC particles are not very stable in the Al melt. For example, Kenndy et al. [30] found that many Al_4C_3 particles were formed after the Al–TiC composite were treated at 700 °C for 48 h. Furthermore, it is suggested that Si element can accelerate the evolution process of TiC in Al melt [31]. If Si content in the Al melt is above 30%, TiC directly reacted with Si and Al to form SiC and $TiAl_xSi_y$ phases [32]. In our previous research work, in-situ SiC particles reinforced Al–Si composited has been prepared utilizing the structural evolution of TiC in the Al–Si melt, which overcoming the difficulties of the low solubility of C element in Al melt and poor wettability between aluminum melt and graphite [32]. It is also found that adding B element in the Al melt can induce the phase transition from TiC to TiB_2, and controlling the transformation from TiC to TiB_2 is found to be an effective method to prepare small and uniform TiB_2 particles [33,34].

In the view of this point, the instability of TiC in the Al melt and its transition induced by certain alloying elements supply facile routes to prepare new materials. It is noticed that Al, Si and B have some similarities with C in the periodic table of the elements, and P is also a near neighbor element of C. Thus, it is necessary to reveal the influence of P on the instability of TiC in the Al melt. In the present study, the transition behavior of TiC in Al–P melt and reactive synthesis of the $Ti_5P_{3.16}$ crystals has been firstly studied. Then, a new Al–Ti–P–C alloy containing the $Ti_5P_{3.16}$ phase was successfully fabricated utilizing the reaction between TiC particles and P atoms. The synthesis process was also revealed based on the crystal morphology evolution of $Ti_5P_{3.16}$ during the reaction using a particle extraction method. The application of the Al–Ti–P–C master alloy on the refinement of the primary Si in A390 alloy was evaluated. Furthermore, the refinement mechanism was also analyzed based on the transition behavior of the $Ti_5P_{3.16}$ in Al–Si melt.

2. Experimental procedures

2.1. Preparation of Al–Ti–P–C master alloy

Commercial pure Al (99.7%, all compositions quoted in this work are in wt. % unless otherwise stated), pure Ti (99.9%), Al–4Ti–1C (i.e. Al–5TiC) alloy, Al–3B alloy, Al–3.5P alloy were used in this experiment. The latter three alloys were supplied by Shandong Al & Mg Melt Technology Co. Ltd. Firstly, Al–3.5P master alloy was melted in clay-bonded graphite using 25 kW medium frequency induction furnaces. The melts were held for 15 min after adding certain amounts of pure Ti, Al–4Ti–1C and Al–3B master alloys at a temperature of about 1300–1400 °C. Thus, a novel Al–8Ti–2.5P–0.5C master alloy with trace B was obtained. The purpose of adding pure Ti and Al–B was to promote the reaction of TiC and P in the melt. Subsequently, the melts were poured into a "U" type permanent mould.

2.2. Refinement tests of Al–Ti–P–C master alloy on A390 alloy

The refinement tests were carried out on A390 alloy supplied by Shandong Al & Mg Melt Technology Co. Ltd and the composition was listed in Table 1. Firstly, A390 alloy was melted in a clay bonded graphite crucible heated by an 25 kW medium frequency induction furnace at 780 °C and the melt was degassed with C_2Cl_6 for 15 min. Then, Al–8Ti–2.5P–0.5C and Al–3.5P master alloy were added into the melt with an addition of 1.5% and 1.0%, respectively. After holding for different times (5 min, 10 min, 15 min, 40 min, 90 min), the melt was poured into a pre-heated mould (150 °C, 70 mm × 35 mm × 20 mm). For comparison, another group samples without P addition were also prepared by the same method. All samples of A390 alloys were poured into the same cast-iron mould at the same casting temperature and subjected to the same cooling rates. The composition of the A390 alloys after refined by the above two master alloys holding for 60 min were also detected and listed in Table 1, indicating that the experimental levels of P in the refined A390 alloys are the same within the margin of error.

2.3. Extraction of Ti-P crystals from Al–Ti–P–C master alloy

In order to clearly observe the crystal morphologies of phases in the Al–8Ti–2.5P–0.5C master alloy, the bulk samples were dissolved in a 10 vol % HCl–distilled water solution to remove the Al matrix. Then, the solutions containing the remaining particles were centrifuged by a centrifugal extractor. After that, the collected sedimented particles were rinsed with distilled water and ethanol for several times and then desiccated for further scanning electron microscope and transmission electron microscope characterization.

2.4. Characterization of the macrostructures of A390 alloy

Metallographic specimens of A390 alloys were cut from the centre part of the casting samples, then mechanically ground and polished with the nano-diamond powder. The average size of the primary Si particles was calculated using the Image-Pro software based on the macrostructure images taken by a high scope video microscope (HSVM, KH–2200), and a least 10 different metallographic specimens were used. Firstly, 30 primary Si particles were chosen and the average area of these particles was measured by the software. Then, the equivalent average size of primary Si particles was determined by the following formula:

$$d = 2^*\sqrt{A/\pi} \quad (1)$$

where A is the average area of primary Si calculated by the software.

2.5. Characterization of microstructures of the alloys and the extracted particles

Phases analysis of the alloys and the extracted Ti-P particles was performed by X-ray diffraction (XRD) recorded on a Rigaku D/max-rB diffractometer equipped with Cu Kα radiation (λ = 1.5418 Å). The microstructure, the morphologies and chemical compositions of the particles were investigated by field emission scanning electron microscope [SEM, Quanta 250F, operated at 15 KV equipped with

Table 1
Chemical composition of A390 alloys (wt.%).

Samples	Si	Cu	Mg	Fe	Zn	Ti	P	Al
A390	17.21	4.58	0.52	0.11	<0.001	0.003	<0.0001	Bal.
A390 + 1.5%Al-8Ti-2.5P-0.5C	17.15	4.45	0.51	0.16	<0.001	0.081	0.209	Bal.
A390 + 1% A-3.5P	17.26	4.51	0.55	0.16	<0.001	0.005	0.203	Bal.

energy-dispersive X-ray spectroscopy (EDS)]. The crystal structure of the $Ti_5P_{3.16}$ particles was characterized directly by transmission electron microscope (TEM, Tecnai20, operated at 200 KV).

3. Results and discussion

3.1. Reactive synthesis of $Ti_5P_{3.16}$ in Al–Ti–P–C melt

Fig. 1 shows the XRD patterns of the Al–3.5P, Al–4Ti–1C, Al–8Ti–2.5P–0.5C master alloy and the extracted particles from the last one, respectively. As shown in Fig. 1(a) and (b), it indicates that AlP and TiC phases are contained in the Al matrix of Al–3.5P and Al–4Ti–1C alloy, respectively. However, the peaks of TiC and AlP phases disappear after the Al–Ti–C added into the Al–P alloy as illustrated in Fig. 1(c), and then $TiAl_3$ and $Ti_5P_{3.16}$ phases are generated in the Al–Ti–P–C alloy indicating that the phase transformation of TiC occurred after added into the Al–P melt. According to the XRD patterns shown in Fig. 1(d), it can be found that the characteristic peaks match well with the JCPDS card (No. 73-1816, Hexagonal $Ti_5P_{3.16}$ with a lattice constant $a = 0.7222$ nm, $c = 0.5093$ nm), which indicates that large amount of $Ti_5P_{3.16}$ particles were successfully synthesized under the present experimental conditions. Besides, a small amount of TiC and TiB_2 phases are also retained in the alloys. Based on the interplaner spacing value detected in diffraction peaks, the lattice parameters *a* and *c* can be calculated using the following formula:

$$d = \frac{1}{\sqrt{\frac{4}{3}\left(h^2 + hk + k^2\right)/a^2 + l^2/c^2}} \quad (2)$$

where d is the interplaner spacing, *h, k* and *l* are indices of the crystallographic planes. Using the values of *h, k, l* and *d* corresponding to diffraction peaks of Ti-P particles, the parameters *a* and *c* can be obtained. The calculated parameters of *a* and *c* are 0.7292 nm and 0.5096 nm, respectively. Compared with the standard data for $Ti_5P_{3.16}$ mentioned above, it can be found that the values of *a* and *c* are slightly increased for the received $Ti_5P_{3.16}$.

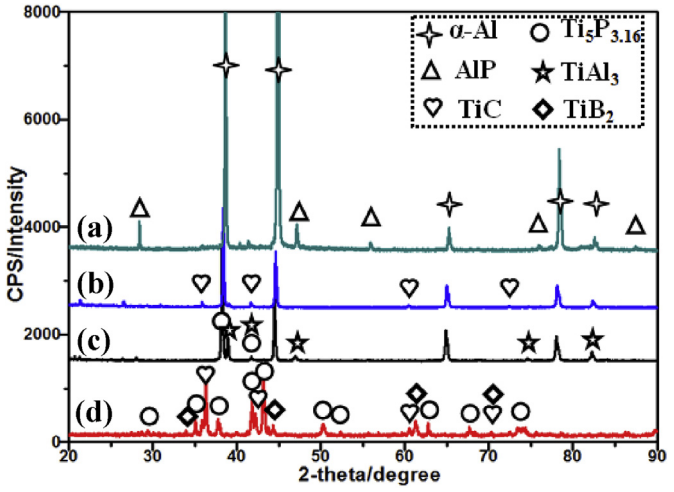

Fig. 1. XRD patterns for the alloys: (a) Al–3.5P; (b) Al–4Ti–1C; (c) Al–8Ti–2.5P–0.5C; (d) extracted particles from (c).

Typical microstructure of the Al–4Ti–1C master alloy is illustrated in Fig. 2(a) and amounts of TiC particles with sizes of about 0.5–3 μm were uniformly distributed in the Al matrix. As shown in Fig. 2(b), it can be seen that the phases in the matrix of Al–Ti–P–C master alloy present two different morphologies–block-like and plate-like. According to the EDS patterns, the plate-like phase can be identified as $TiAl_3$. Meanwhile, the light block-like particle of 10–20 μm in size containing Ti and P elements is confirmed to be $Ti_5P_{3.16}$ (Fig. 2(c and d)). Besides, a small amount of dark AlP particles with 3–5 μm in size can be seen in the Al matrix indicated by the arrow, which are the residual particles from Al–P alloy. Thus, AlP peaks are not shown obviously because of the relatively low content. While, the excess P content is benefit to the transformation from TiC to $Ti_5P_{3.16}$. It is noticed from Fig. 2(c) that the flakes adhering to $Ti_5P_{3.16}$ particles are also $TiAl_3$ phase, and some TiC and TiB_2 particles with sizes about 0.5–2 μm can be seen in the matrix.

3.2. Crystal morphology of $Ti_5P_{3.16}$ particles

Fig. 3 shows the three-dimensional crystal morphologies of the particles extracted from the Al–Ti–P–C alloy. It can be seen that most of the particles are regular hexagonal prisms as shown in Fig. 3(a and b). The length of the basal plane of these hexagonal prisms ranged from 5 to 15 μm and the height ranged from 10 to 20 μm. According to the EDS patterns for a typical prism (Fig. 3(a) and (c)), it proves that the hexagonal shape particles are $Ti_5P_{3.16}$. It is also noted that the C peak also appears, and it is considered that a trace amount of C atoms may be remained in the interstitial sites of $Ti_5P_{3.16}$ and some C impurity atoms from the SEM beam deposited on the particle surface, leading to the increase of C content. Fig. 4 illustrate the HRTEM images of a hexagonal $Ti_5P_{3.16}$ platelet and the corresponding selected-area electron diffraction (SAED) obtained by directing the electron beam perpendicular to one of the basal planes. Calculation from the lattice image of Fig. 4(b) shows that the interplaner crystal distance is ~0.313 nm, which corresponds to the crystal plane (2 0-2 0) of $Ti_5P_{3.16}$. The SAED patterns with [0001] axis as shown in the inset of Fig. 4(b) indicate that the $Ti_5P_{3.16}$ hexagonal platelet has a typical h.c.p crystal lattice structure and displays the hexagonal prism morphology with two parallel {0001} facets and six {10-10} ones.

3.3. Formation process of the $Ti_5P_{3.16}$ in the Al–Ti–P–C alloy

The FESEM images shown in Fig. 5 provide clear information about the typical morphologies at different growth stages of Ti–P phase in the Al–Ti–P–C alloy. As shown in Fig. 5(a), it shows that lots of TiC particles are agglomerated to form compacted clusters and some individual TiC hexagonal plates also exist as shown in the inset of Fig. 5(a). According to the EDS patterns of point A shown in Fig. 5(e), it can be seen that trace P atoms absorbed on the TiC agglomeration at the initial stage. It is believed that the transformation started after increased more P atoms diffuse into the crystal structure of TiC. As shown in Fig. 5(b), it is a typical

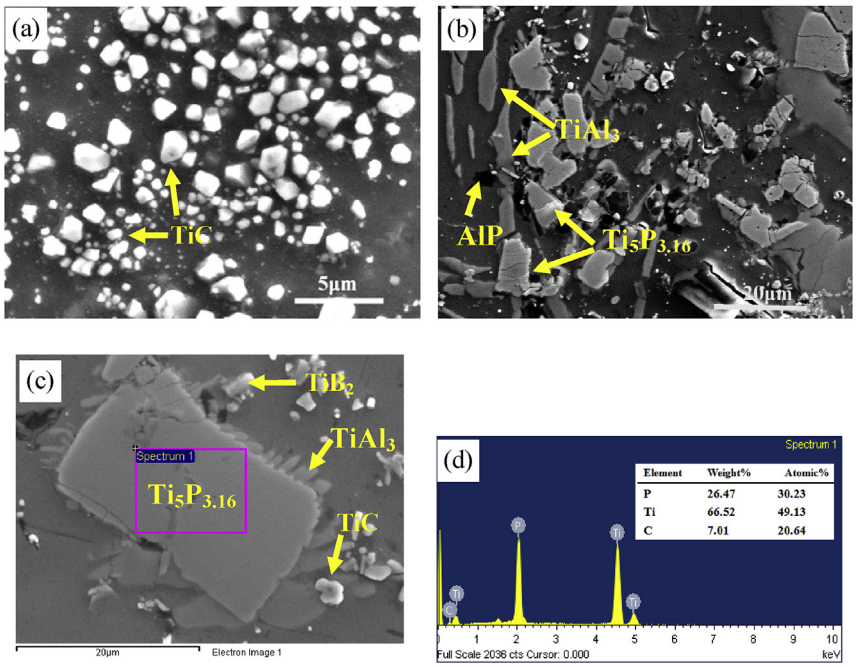

Fig. 2. FESEM micrographs of the prepared master alloys: (a) SEI image of the Al–4Ti–1C showing the morphology and distribution of TiC particles; (b) SEI images of the Al–8Ti–2.5P–0.5C indicating the distribution of the phases; (c) higher magnification revealing the morphology and size of $Ti_5P_{3.16}$; (d) EDS spectra of corresponding area in (c).

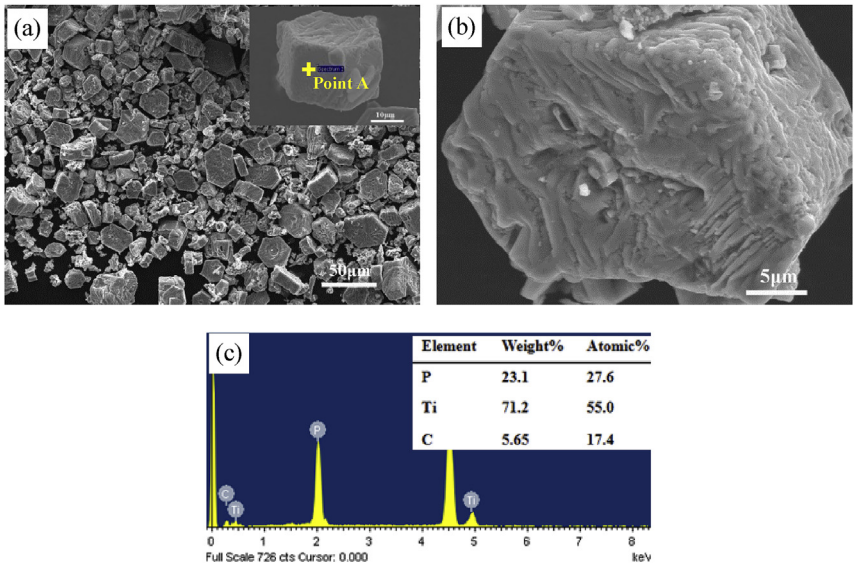

Fig. 3. Typical morphologies of the extracted particles from Al–Ti–P–C master alloy: (a–b) SEI images of $Ti_5P_{3.16}$; (c) the corresponding EDS analysis for point A in set of (a).

morphology during the transition state with a half TiC agglomerates and the other half Ti-P phase. It is proposed that the absorption and accumulation of P atoms promoted the transition from TiC to Ti-P phase. With the gradual proceeding of the phase evolution, more P atoms diffused into the interstitial structure of TiC and then the C atoms diffused out. According to the EDS point analysis as shown in Fig. 5(e)-(g), it is clearly observed that the concentration of P in the particles increased gradually. Based on the above analysis, it is proposed that the following reaction occurred.

$$TiC_{(s)}+[P]+ Al_{(l)} \rightarrow Ti\text{-}P_{(s)}+Al_4C_{3(s)} \quad (3)$$

It is worthwhile to note that some hollows can be observed on the Ti-P phase at the transition state. According to the crystal growth study on the intermetallic compounds in the literatures, hopper is typical characteristic during the crystal growth and morphology evolution process [35–37]. It is considered that the hopper growth began much earlier due to the cooling rate being low and therefore it is usually formed at the early growth stage as evidenced by Fig. 5(c). With time prolonged, to reduce the total surface energy of the hole crystal, the base of the hopper will be gradually filled by the slower growing facets as shown in Fig. 5(c) and then a complete hexagonal crystal of Ti-P phase is formed (Fig. 3(b)). Actually, the growing rates of each facets are influenced by many factors, especially the specific surface energy of each crystal plane for the Ti-P phases and the solute elements in the

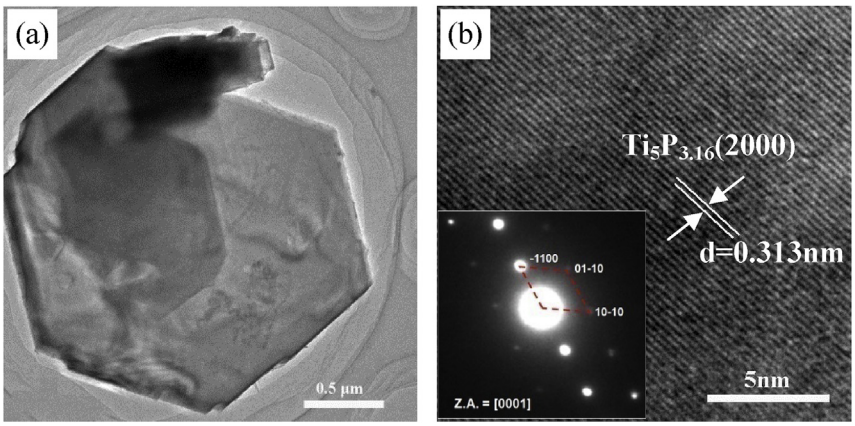

Fig. 4. TEM analysis of extracted $Ti_5P_{3.16}$ crystal: (a) morphology; (b) corresponding SAED pattern and lattice image.

melt, which needs to be addressed in detail in the future investigation.

Because the preformed TiC particles usually agglomerated with a size larger than 5 μm, the Ti-P crystal also has a size larger than 10 μm. From this point of view, it may be a facile method to control the size of Ti-P crystals by reducing the size and agglomeration of TiC particles. It is also noted that a residual TiC hexagonal platelet embedded on the surface of the Ti-P crystal as shown by the arrow in Fig. 5(d). According to the EDS patterns of the hexagonal crystal as illustrated in Fig. 5(h), it was further confirmed to be the $Ti_5P_{3.16}$.

3.4. Application of Al–Ti–P–C master alloy on Si refinement of A390 alloy

Refinement tests were carried out to evaluate the refinement efficiency of the Al–Ti–P–C master alloy bearing $Ti_5P_{3.16}$ on hypereutectic Al–Si alloys. Fig. 6(a–d) show the as-cast microstructures of A390 alloys without and with the addition of 1.5% Al–8Ti–2.5P–0.5C master alloy (P addition about 209 ppm). Meanwhile, the refining efficiency of Al–Ti–P–C master alloy is compared with that of Al–P master alloy (Fig. 6(e)-(h)). As illustrated in Fig. 6(a), the average grain size of coarse primary Si in unrefined A390 alloys is about 85 μm. The Al–Ti–P–C master alloy leads to a significant increase in the number density of primary Si and a drastic decrease of the size of primary Si after holding for only 5 min as shown in Fig. 6(b). Therefore, A390 alloys have shown a fast refinement response to the addition of Al–Ti–P–C master alloy. When the holding time was increased to 15 min, primary Si particles were refined further as illustrated in Fig. 6(c) and the good refinement was also obtained even at 90 min holding (Fig. 6(d)), indicating that the Al–Ti–P–C master alloy behaves a good fading resistance. It is noted that the microstructure of eutectic Si in the Al matrix is significantly refined as well. Compared with the grain refining efficiency of Al–P master alloy with the P addition of about 203 ppm as shown in Fig. 6(e)-(f), it can be seen that the Al–Ti–P–C master alloy shows a higher refining efficiency and the average size of primary Si particles is much smaller. Compared with the commonly used Cu–P master alloy [38], the Al–Ti–P–C master alloy also shows a much better grain refinement performance.

Fig. 7 definitely illustrates the variation trend of the average size of the primary Si particles as the holding time. It shows that the average grain size of primary Si is evidently reduced from about 85 μm to nearly 18.5 μm when 1.5% Al–8Ti–2.5P–0.5C master alloy is added after holding for 5 min. With an increased holding time to 15 min, the average size of primary Si is further reduced to 12.5 μm due to the increased more nucleating sites were formed in the melt. With time prolonged to 90 min, the good grain refining performance can be kept as well, indicating that the master alloy behaves a good fading resistance. After adding 1% Al–3.5P master alloy, the smallest average particle size of primary Si is about 20 μm obtained after holding for 15 min. Compared with the refining curve of the Al–P master alloy, the average particle size of primary Si refined by the Al–Ti–P–C master alloy is much smaller and a higher refining efficiency is obtained. Furthermore, it can be concluded that the Al–Ti–P–C master alloy refines primary Si particles more quickly and more stable than the Al–P alloy.

Fig. 8 shows the SEI images of A390 alloys refined by the Al–Ti–P–C master alloy and three kinds of phases—black primary Si, eutectic Si and white Cu-rich phase—can be seen in the Al matrix. It is clear that the average size of primary Si particles decreased dramatically after 15 min holding as shown in Fig. 8(a) and the good refinement performance can be kept with the increase of holding time for 40 min as shown in Fig. 8(b). Therefore, it can be concluded that the new Al–Ti–P–C master alloy is a highly efficient refiner for hypereutectic Al–Si alloys with good fading resistance. It is noticed that a dark phase was often observed in the centre of primary Si particles and the typical example is marked by yellow arrow in Fig. 8, which has been investigated and is believed to be AlP in our previous study [12].

3.5. Refinement mechanism of primary Si by $Ti_5P_{3.16}$ phase

Why does Al–Ti–P–C master alloy containing $Ti_5P_{3.16}$ phase display the good refinement performance on A390 alloys? Up to now, there is no literature about the synthesis of $Ti_5P_{3.16}$ phase in the Al–Ti–P alloy and its refinement mechanism on the primary Si phase. It was reported that ZrP could react with Si atom clusters in the Al melt to form AlP particles [9], and then the AlP particles acted as good nucleating substrates for primary Si during solidification [15,39].

In order to explore the phase evolution of $Ti_5P_{3.16}$ and its refinement mechanism on primary Si, 15% Si was added into the Al–Ti–P–C master alloy. Compared the microstructures of Al–Ti–P–C–Si shown in Fig. 9(a and b) and those of Al–Ti–P–C shown in Fig. 2(b), it can be seen that most of $Ti_5P_{3.16}$ particles disappear and two new phases appeared in the Al matrix after the addition of Si. According to the EDS analysis in Fig. 9(c), the large blocky phase contained Al, Ti and Si elements is likely to be a (Al,Ti,Si) phase, and the dark phase adhered to the (Al,Ti,Si) phase contained Al, P and O. It has been demonstrated that the distribution of O is likely to correspond with the P distribution, which appears to be due to a rapid-oxidation event of the P-rich particle

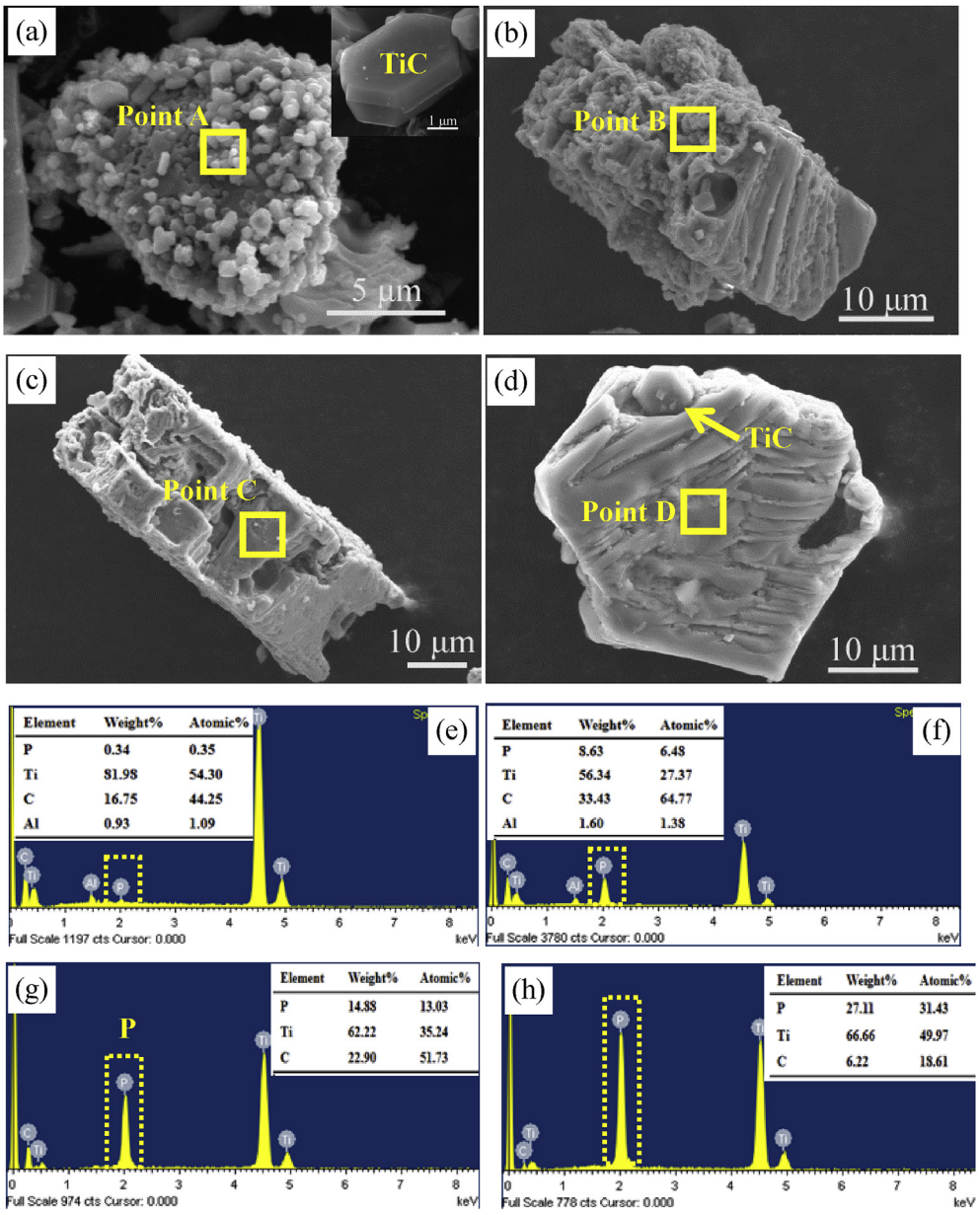

Fig. 5. Typical morphologies of Ti-P phase at different growing stage in the Al–Ti–P–C system: (a) TiC agglomerates; (b,c) transition states of Ti-P phase; (d) hexagonal $Ti_5P_{3.16}$ with hopper; (e–h) EDS patterns for points A-D.

[40]. As we know, AlP is unstable in air during sample preparation and reacts with water as follows:

$$AlP(s)+3H_2O(g) \rightarrow Al(OH)_3(s)+PH_3(g) \quad (4)$$

Therefore, it is reasonable to believe that the dark phase is the hydrolyzed AlP particle. The released P from the Ti-P phase will combine with surrounding Al atoms and form large AlP particles due to the very low solubility of P in the Al matrix. Based on the above analysis, it is deduced that the phase transition of $Ti_5P_{3.16}$ is induced by the Si atoms and the reaction can be described as follows:

$$Ti_5P_{3.16}(s) + [Si] + Al(l) \rightarrow (Al, Ti, Si)(s) + AlP(s) \quad (5)$$

Furthermore, Fig. 10 shows a typical microstructure of the transition zone surrounding the $Ti_5P_{3.16}$ particle. The white $Ti_5P_{3.16}$ particle in the centre was doped with trace Si atoms as shown in Fig. 10(b), while the gray coral-like phase surrounding the centre particle was the (Al,Ti,Si) phase. It is obvious that the transition started from the outer interface and then proceeded gradually to the centre part. It is worthy to note that the black nano AlP particles with sizes about 100–200 nm are embedded in the (Al,Ti,Si) phase. Therefore, it is considered that after the Al–Ti–P–C master alloy is added into A390 melt, Si atoms will induce the gradual transition of the Ti-P phase along with the formation of amounts of nano AlP particles.

Based on the above discussion, a diffusion controlled model is proposed to illustrate the phase transition processes of $Ti_5P_{3.16}$ phase in the Al–Si melt as shown in Fig. 11. After Si is added in the Al–Ti–P–C melt, Si atoms dissolve in the Al melt firstly and then absorb on the surface of $Ti_5P_{3.16}$ particles. When more Si atoms

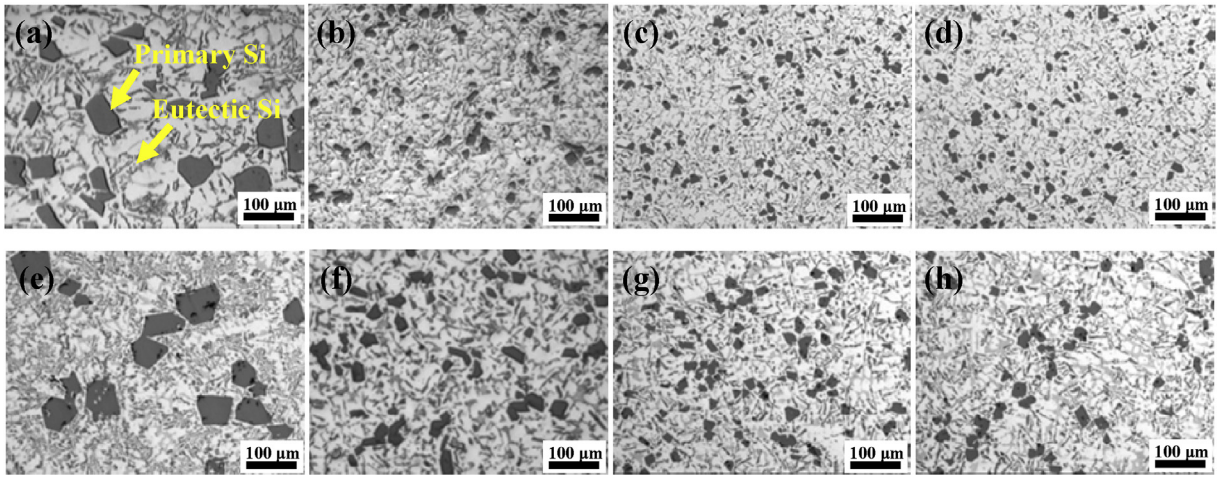

Fig. 6. Typical microstructures of A390 alloy before and after refinement: (a, e) unrefined; (b–d) adding 1.5% Al–8Ti–2.5P–0.5C master alloy at 780 °C with 5, 15 and 90 min holding, respectively; (f–h) adding 1% Al–3.5P master alloy at 780 °C with 5, 15 and 90 min holding.

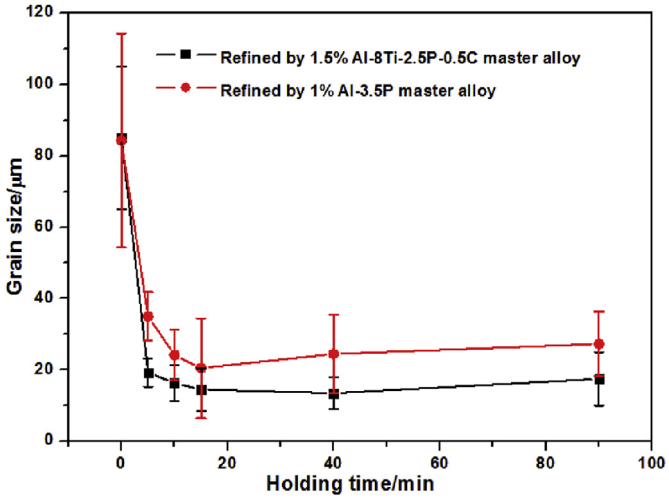

Fig. 7. Refining performances of Al–Ti–P–C and Al–P master alloys on primary Si in A390 alloys.

diffuse towards and aggregate on the surface, the solid-liquid reaction between $Ti_5P_{3.16}$ phase and Si atoms starts from the out layer, and then (Al,Ti,Si) phase forms surrounding the Ti-P particles as shown in Fig. 11(b). Because the solubility of P in the Al melt is very low [41], the released P atoms will directly combine with Al atoms to form nano sized AlP particles. Therefore, it is believed that the entire reaction process is controlled by the gradual diffusion of Si and Al atoms in the Ti-P phase from the outer layer to the inner part. Finally, after debonding from reaction interface, AlP particles and (Al,Ti,Si) compounds grow up and then distribute evenly in matrix as shown in Fig. 11(c).

Crystallization nuclei of primary Si refined by the Al–Ti–P–C master alloy were analyzed as shown in Fig. 12(a). Due to the hydrolyzation of the AlP particles, it is often very difficult to obtain the direct nuclei of primary Si. Herein, the elemental mapping analysis was carried out on the whole surface of the primary Si as shown in Fig. 12(a). Although no visible particle appears on the surface, the EDS elemental mapping patterns (Fig. 12(b–d)) proves that a phase containing Al and P was located in the inner centre of the Si particles. Furthermore, the EDS point analysis (Fig. 12(e)) also shows that the P: Al atomic ratio of the phase is about 1:1. Thus, it can be concluded that the nucleus is AlP, due to that primary Si nucleates heterogeneously on the solid AlP particles with a cube-cube orientation relationship for they are both diamond cubic with similar lattice parameters [14,38]. Therefore, it can be concluded that the Si atoms induced the phase transition from $Ti_5P_{3.16}$ to AlP in Al melt, and then these in-situ AlP particles can act as the highly efficient heterogeneous nucleating sites for the primary Si during the solidification process.

It is known that P content in normal commercial-purity Al–Si alloys is often less than 10 ppm [42,43]. When the value of P level in the melt is low, the number of AlP particles acting as potent nucleants will be limited in the melt and then primary Si particles cannot be refined effectively. Therefore, it has an optimum content for P to obtain an effective refinement for primary Si in Al–Si melt. It is found that the effective refinement can be obtained when P

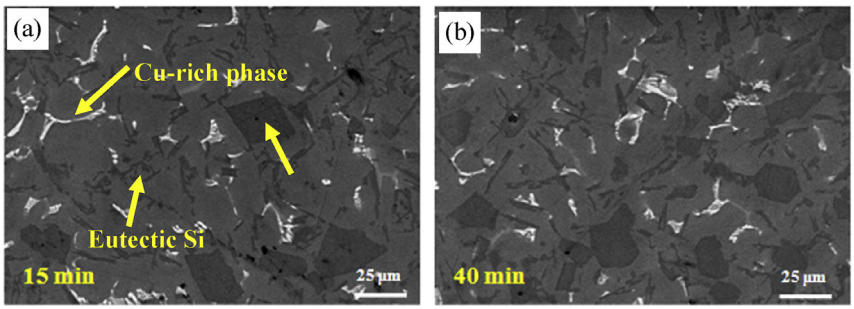

Fig. 8. The microstructures of A390 alloy refined by the Al–Ti–P–C master alloy at a higher magnification: (a, b) the SEI images after holding for 15 min and 40 min, respectively.

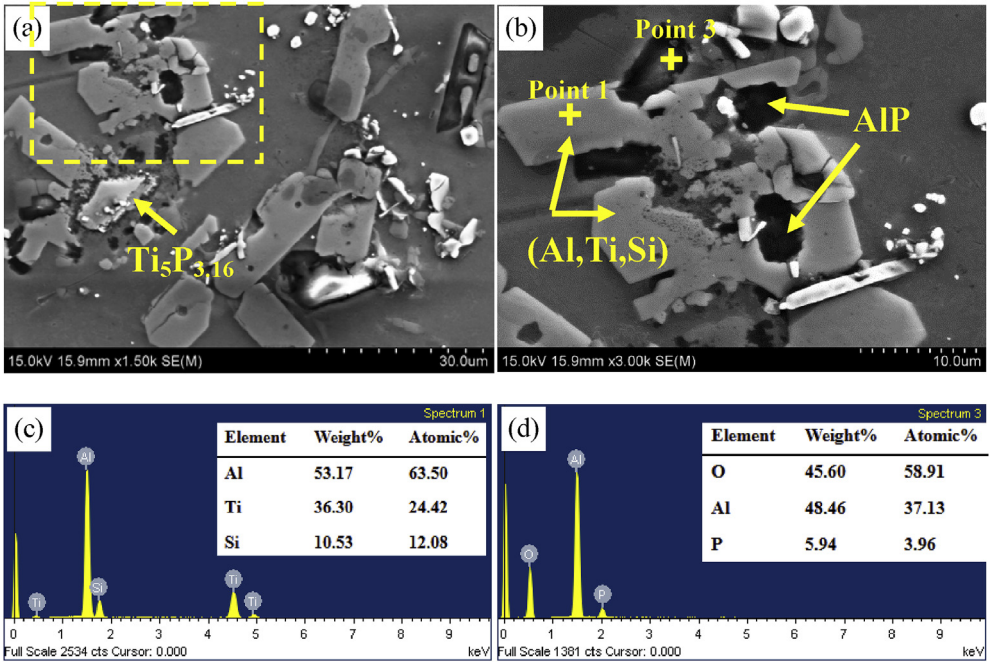

Fig. 9. Microstructures of Al–8Ti–2.5P–0.5C–15Si alloy: (a–b) SEI images; (c–d) EDS patterns of Point 1 and 3.

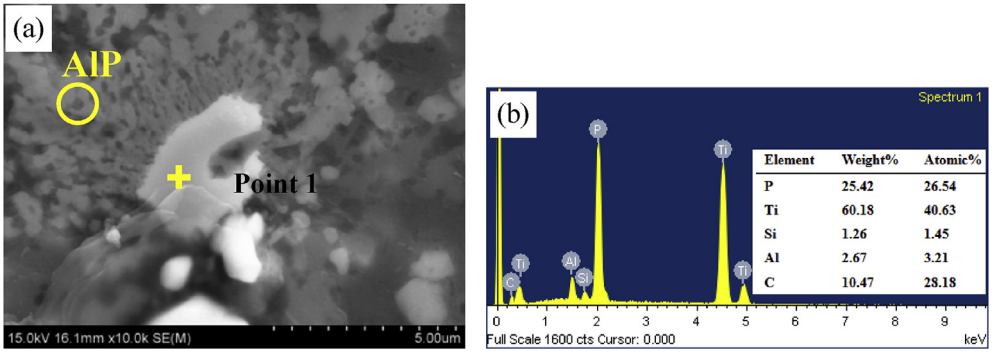

Fig. 10. Typical microstructure surrounding $Ti_5P_{3.16}$ particles in Al–8Ti–2.5P–0.5C–15Si system: (a) SEI image; (b) EDS Patterns of point 1.

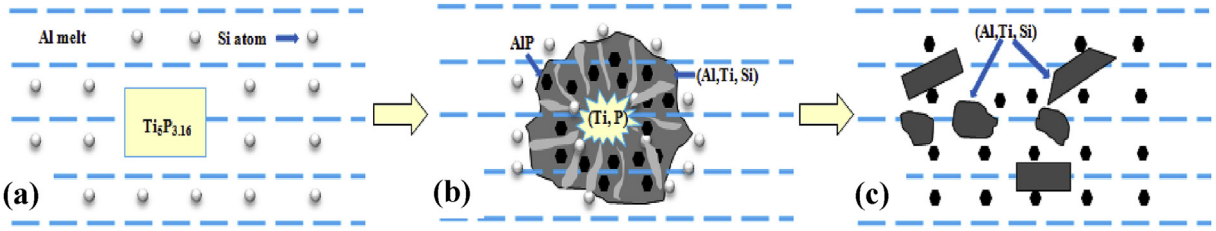

Fig. 11. Schematic illustration of the evolution processes of $Ti_5P_{3.16}$ phase in Al–Si melt.

content in the melt is above 100 ppm. Due to the P loss during the casting, the addition of P should be more than 200 ppm.

According to the literatures [44,45], it is known that the morphology, size, interface, distribution and quantity of the nucleant particles have major impacts on the grain refining efficiency. With increase of the quantity, decrease of the size and improvement of the interface of the nucleation particles, the refining efficiency will be better. Most of the added AlP particles in the master alloy or in-situ formed in the melt are single crystals and will be uniformly distributed in the Al–Si melt. Therefore, only one dark AlP phase was observed at the centre of primary Si particles in the present experiment condition. When P content is increased to some extent, few AlP particles may be agglomerated into particle clusters to act as nuclei, which were not observed in the experiment.

Fig. 13 (a) shows a microstructure of Al–3.5P master alloy and most of the AlP particles have an average size larger than 20 μm. Due to the oxidation of AlP in air, the element O is also detected as

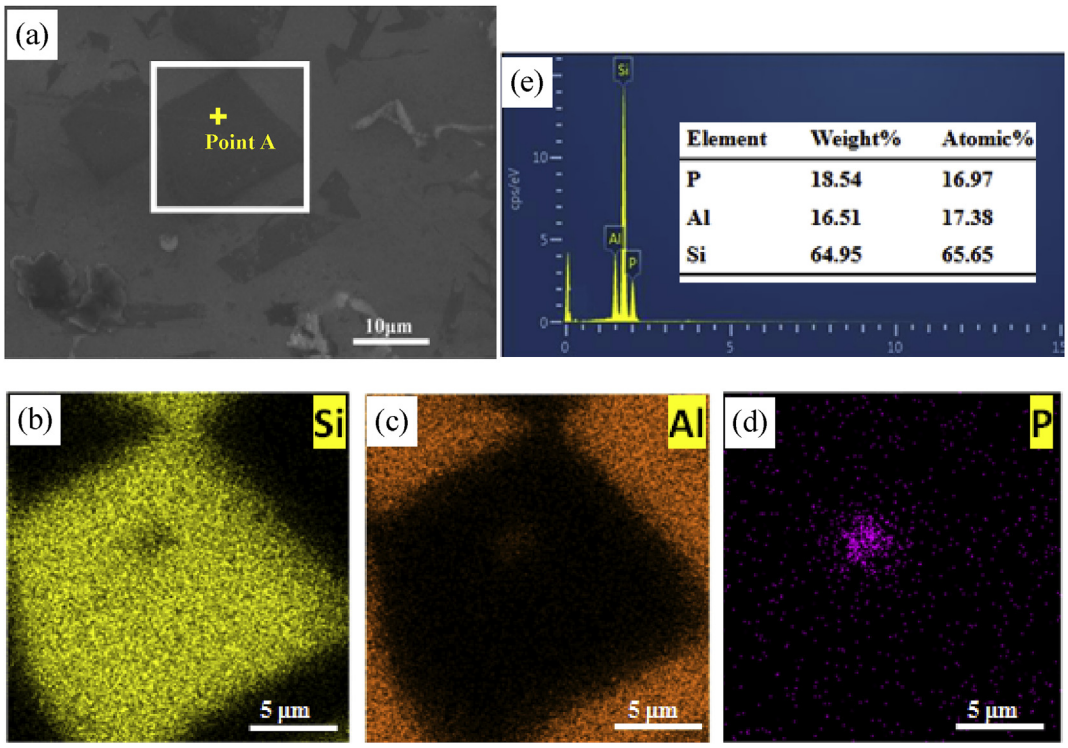

Fig. 12. Microstructure and elemental mapping micrographs for primary Si in A390 alloys refined by Al–Ti–P–C master alloy: (a) SEI image, (b–d) mapping micrographs for Si, Al and P elements, (e) EDS patterns of point A.

shown in Fig. 13(b). After the Al–P alloy added into the Al–Si melt, the pre-exist AlP particles gradually start to dissolve and smaller sized in-situ AlP will precipitated with the temperature decreasing during solidification. However, due to the lower solubility of P, the re-precipitation process is restricted by the equilibrium constant of the dissolution reaction AlP(s)→[Al] +[P], and a large quantity of AlP particles cannot dissolved in the melt, which leads to the reduced number of effective nucleating site [18]. Furthermore, the solubility and precipitation of AlP in Al–Si melts were studied with a temperature controlled filtration technique, indicating that it would take a very long time about more than 20 h to reach the P equilibrium solute concentration [38]. Therefore, the number of effective nucleating AlP substrates for primary Si is limited after the Al–P alloys added into the Al–Si melt and the nucleation rate is relatively low.

In comparison, after the Al–Ti–P–C alloy added into the Al–Si melt, the transformation reaction of $Ti_5P_{3.16}$ will be induced rapidly by Si atoms in the melt and then amounts of nano and sub-micron sized AlP nucleating particles with fresh interface will formed in a short time. With the temperature decreasing during solidification, these in-situ AlP particles will act as the nucleating substrates for the primary Si. A large number of efficient nuclei are available for the primary Si, so the quantity of the primary Si increases significantly, and accordingly the size decrease. The nucleation rate of the Al–Ti–P–C master alloy is promoted due to the increased nucleating sites, leading to the improvement of the refining efficiency. In addition, it has been mentioned in Fig. 2 that small amount of TiC and TiB_2 particles are also remained in the master alloy, which are proved to have a favorable effect on the improvement of the phosphorous modification efficiency in the previous study [46–49]. It is found that TiB_2 particles are the good nucleation substrate for AlP compound and the trace addition of TiC particles can significantly increase the absorptivity of P in the melt, greatly improving the modification effect [46,47]. Therefore, the

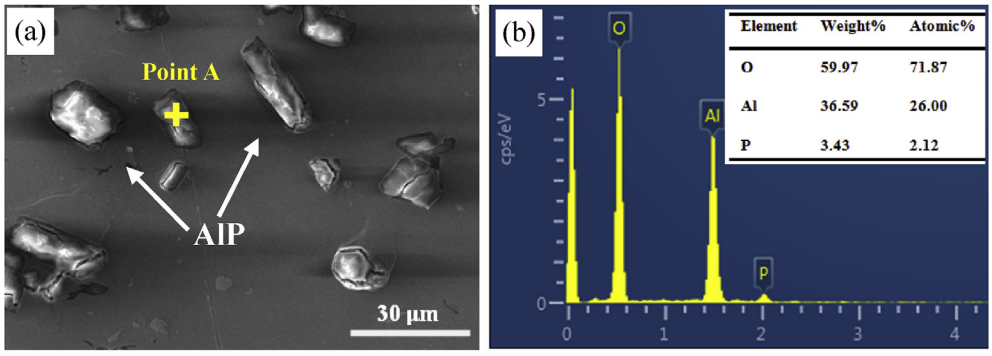

Fig. 13. Microstructure of Al–3.5P master alloy (a) and EDS point analysis of AlP (b).

Al–Ti–P–C mater alloy behaves a better refinement performance on the A390 alloy than the Al–P alloy and is a promising refiner for the hypereutectic Al–Si alloys.

4. Conclusions

In this work, the reactive synthesis of $Ti_5P_{3.16}$ particles in the Al–Ti–P–C alloy and it is application on refinement of the primary Si particles in the Al–Si alloys have been systematically studied. The main results are summarized as follows:

(1) The $Ti_5P_{3.16}$ phase was formed by the solid-liquid reaction of TiC particles with solute P atoms. During the reaction process, P atoms absorbed on the surface of the TiC particles firstly and initiated their gradual decomposition, and then P and Ti atoms combined together to form the Ti-P phase. The $Ti_5P_{3.16}$ phase has an hexagonal close packed crystal lattice structure and mainly displays the regular hexagonal prism morphology enclosed by six {10-10} facets and two parallel {0001} facets.

(2) The Al–Ti–P–C master alloys containing $Ti_5P_{3.16}$ phase displayed a better and more stable refining performance on the primary Si particles in the A390 alloy, compared with the Al–P alloys. The average size of the primary Si particles was dramatically reduced from 85 μm to 12.5 μm by the addition of 1.5% Al–8Ti–2.5P–0.5C master alloy.

(3) The refinement mechanism of the primary Si can be revealed based on the phase transition behavior of the $Ti_5P_{3.16}$ in the Al–Si melt. It is believed that Si atoms diffuse towards the $Ti_5P_{3.16}$ surface and induce the gradual transformation along with the formation of amounts of nano and sub-micron AlP particles, which will be the efficient heterogenous nuclei for the primary Si. Because the transformation process will not be limited by the equilibrium constant of the dissolution and precipitation reaction of AlP in the Al–P master alloy, a smaller primary Si size can be obtained for the Al–Ti–P–C master alloy.

Acknowledgments

This research was financially supported by the National Natural Science Foundation of China (Nos. 51731007, 51501092 and 51571133). We also acknowledge the support of the Jiangsu Key Laboratory of Advanced Micro-Nano Materials and Technology.

References

[1] J.R. Davis, et al., ASM Handbook: Casting, third ed., vol. 15, ASM International, Metals Park, OH, 1998, pp. 751–753.
[2] J. Li, M. Elmadagli, V.Y. Gertsman, J. Lo, A.T. Alpas, Mater. Sci. Eng. A 421 (2006) 317–327.
[3] M.M. Haque, A. Sharif, J. Mater. Process. Technol. 118 (2001) 69–73.
[4] V.C. Srivastava, R.K. Mandal, S.N. Ojha, Mater. Sci. Eng. A 383 (2004) 14–20.
[5] C.L. Xu, Q.C. Jiang, Y.F. Yang, J. Alloys Compd. 422 (2006) L1–L4.
[6] J. Chang, I. Moon, J. Mater. Sci. 33 (1998) 5015–5023.
[7] X.F. Liu, J.G. Qiao, Y.X. Liu, S.T. Li, X.F. Bian, Acta Metall. Sin. 40 (2004) 471–476.
[8] Q.C. Jiang, C.L. Xu, M. Lu, H.Y. Wang, Mater. Lett. 59 (2005) 624–628.
[9] W.J. Kyffin, W.M. Rainforth, H. Jones, J. Mater. Sci. 36 (2001) 2667–2672.
[10] M. Zuo, J. Kun, X.F. Liu, J. Alloys Compd. 503 (2010) 26–30.
[11] Y.P. Wu, S.J. Wang, H. Li, X.F. Liu, J. Alloys Compd. 477 (2009) 139–144.
[12] J.H. Li, F.S. Hage, X.F. Liu, Q. Ramasse, P. Schumacher, Sci. Rep. 25244 (2016) 1–7.
[13] S.M. Liang, R. Schmid-Fetzer, Acta Mater. 72 (2014) 41–56.
[14] C.R. Ho, B. Cantor, Acta Metall. Mater. 43 (1995) 3231–3246.
[15] C. Li, X.F. Liu, Y.Y. Wu, J. Alloys Compd. 465 (2008) 145–150.
[16] K. Nogita, S.D. McDonald, K. Tsujimoto, K. Yasuda, A.K. Dahle, J. Electron Microsc. 53 (2004) 361–369.
[17] E.A. Brandes, C.J. Smithells (Eds.), Metals Reference Handbook, Butterworth, London, 1983, pp. 6–29.
[18] M. Zuo, X.F. Liu, Q.Q. Sun, K. Jiang, J. Mater. Process. Technol. 209 (2009) 5504–5508.
[19] X.F. Liu, J.G. Qiao, X.G. Song, X.F. Bian, L.M. Zhu, Y.L. Zhang, Spec. Cast. Nonferrous Alloy 6 (2002) 43–45.
[20] G.J. Bao, M. Zuo, D.K. Li, Y.G. Li, X.F. Liu, Mater. Sci. Eng. A 531 (2012) 55–60.
[21] C.L. Xu, H.Y. Wang, Y.F. Yang, H.Y. Wang, Q.C. Jiang, J. Alloys Compd. 421 (2006) 128–132.
[22] M. Zuo, X.F. Liu, J. Inorg. Organomet. Polym. 22 (2012) 64–69.
[23] G.J. Bao, D.K. Li, J.F. Nie, X.F. Liu, J. Alloys Compd. 528 (2012) 45–50.
[24] Q. Zhang, X.F. Liu, H.S. Dai, J. Alloys Compd. 480 (2009) 376–381.
[25] S.K. Bhaumik, C. Divakar, A.K. Singh, G.S. Upadhyaya, Mater. Sci. Eng. A 279 (2000) 275–281.
[26] J.F. Li, F. Li, K. Hu, Y. Zhou, J. Eur. Ceram. Soc. 21 (2001) 2829–2833.
[27] G. Wen, S.B. Li, B.S. Zhang, Z.X. Guo, Acta Mater. 49 (2001) 1463–1470.
[28] G.S. Vinod Kumar, B.S. Murty, M. Chakraborty, J. Alloys Compd. 396 (2005) 143–150.
[29] H.M. Ding, X.F. Liu, L.N. Yu, G.Q. Zhao, Scr. Mater. 57 (2007) 575–578.
[30] A.R. Kennedy, D.P. Weston, M.I. Jones, Mater. Sci. Eng. A 316 (2001) 32–38.
[31] H.M. Ding, H. Li, X.F. Liu, J. Alloys Compd. 485 (2009) 285–289.
[32] J.F. Nie, D.K. Li, E.Z. Wang, X.F. Liu, J. Alloys Compd. 613 (2014) 407–412.
[33] J.F. Nie, Y.H. Zhao, E.Z. Wang, X.F. Liu, Mater. Char. 100 (2015) 68–73.
[34] H.M. Ding, X.F. Liu, J.F. Nie, Mater. Char. 63 (2012) 56–62.
[35] C. Li, Y.Y. Wu, H. Li, X.F. Liu, Acta Mater. 59 (2011) 1058–1067.
[36] G. Han, X.F. Liu, Acta Mater. 114 (2016) 54–66.
[37] J.F. Nie, Y.Y. Wu, P.T. Li, H. Li, X.F. Liu, CrystEngComm 14 (2012) 2213–2221.
[38] T. Gao, X.Z. Zhu, H. Qiao, X.F. Liu, J. Alloys Compd. 607 (2014) 11–15.
[39] A.J. Mcalister, J. Phase Equil. 6 (1985) 222–224.
[40] Y.H. Cho, H.C. Lee, K.H. Oh, A.K. Dahle, Metall. Mater. Trans. A 39 (2008) 2435–2448.
[41] H. Lescuyer, M. Allibert, G. Laslaz, J. Alloys Compd. 279 (1998) 237–244.
[42] S.D. McDonald, K. Nogita, A.K. Dahle, Acta Mater. 52 (2004) 4273–4280.
[43] S.D. McDonald, A.K. Dahle, J.A. Taylor, D.H. StJohn, Metall. Mater. Trans. A 35 (2004) 1829–1837.
[44] T.E. Quested, A.L. Greer, Acta Mater. 52 (2004) 3859–3868.
[45] P.L. Schaffer, A.K. Dahle, Mater. Sci. Eng. A 413–414 (2005) 373–378.
[46] Y.F. Han, X.F. Liu, H.M. Wang, Z.Q. Wang, X.F. Bian, J.Y. Zhang, Trans. Nonferrous Met. Soc. China 13 (2003) 92–96.
[47] L.N. Yu, X.F. Liu, H.M. Ding, J. Alloys Compd. 432 (2007) 156–162.
[48] L.N. Yu, X.F. Liu, H.M. Ding, J. Alloys Compd. 429 (2007) 119–125.
[49] X.L. Zhou, Y.Y. Wu, Y.F. Li, L. Wu, T. Gao, H. Li, X.F. Liu, J. Alloys Compd. 693 (2017) 853–858.